Mineral aerosol contamination of TIROS Operational Vertical Sounder (TOVS) temperature and moisture retrievals

C. J. Weaver
University of Maryland, Baltimore County, Baltimore, Maryland, USA

J. Joiner
NASA Goddard Space Flight Center, Greenbelt, Maryland, USA

P. Ginoux
University of Maryland, Baltimore County, Baltimore, Maryland, USA

Received 25 May 2002; revised 11 October 2002; accepted 6 December 2002; published 23 April 2003.

[1] Since mineral aerosols absorb significant amounts of infrared radiation, they may contribute to errors in the retrievals of atmospheric and surface parameters from the TIROS Operational Vertical Sounder (TOVS) High-Resolution Infrared Radiation Sounder (HIRS) if the atmosphere is assumed clear. TOVS is an operational sounder on NOAA polar satellites. To see if observed brightness temperatures are reduced by mineral aerosol, we analyzed results from the Data Assimilation Office (DAO) Finite Volume Data Assimilation System (fvDAS). Every 6 hours the assimilated temperature and moisture profiles are used as a first guess in the DAO interactive cloud-clearing TOVS retrieval system. The observed minus the forecast (O–F) brightness temperature, which is a measure of the accuracy of the first guess and radiative transfer parameters, becomes more negative with increasing dust concentrations. Dust concentrations are from the Goddard Ozone Chemistry Aerosol Radiation Transport (GOCART) model. Since there was no account of dust during this fvDAS run, the dependence of O–F on the estimated atmospheric dust concentrations from GOCART indicates that the dust is affecting the TOVS brightness temperatures. HIRS channels that are sensitive to the surface temperature, lower tropospheric temperature, and moisture are subject to a 0.5 K or more reduction in the brightness temperature during heavy dust loading conditions. The radiative transfer module used in the TOVS retrieval system was modified to account for dust assuming a composition of illite, and the fvDAS run was repeated. Accounting for dust absorption in the retrieval system yields warmer surface temperatures (0.4 K) and warmer lower tropospheric temperatures in regions of moderate dust loading over the tropical Atlantic. *INDEX TERMS:* 6969 Radio Science: Remote sensing; 3337 Meteorology and Atmospheric Dynamics: Numerical modeling and data assimilation; 0305 Atmospheric Composition and Structure: Aerosols and particles (0345, 4801); *KEYWORDS:* TOVS, dust, mineral, aerosol, temperature, retrievals

Citation: Weaver, C. J., J. Joiner, and P. Ginoux, Mineral aerosol contamination of TIROS Operational Vertical Sounder (TOVS) temperature and moisture retrievals, *J. Geophys. Res.*, *108*(D8), 4246, doi:10.1029/2002JD002571, 2003.

1. Introduction

[2] It is well known that atmospheric aerosols can influence cloud properties, change local dynamics, provide catalysts for heterogeneous chemical reactions and impact the Earth's radiation budget. This study investigates an additional potentially important effect: dust contamination of satellite-sensed temperature and moisture. We consider the High-Resolution Infrared Radiation Sounder (HIRS) radiances that is part of the TIROS Operational Vertical Sounder (TOVS). The TOVS and Advanced TOVS (ATOVS), which fly on NOAA polar operational environmental satellites (POES) are the only long-term source of high-spatial resolution global information pertaining to the temperature and moisture structure of the atmosphere. Since the TOVS radiances have widespread use in weather forecasting and data assimilation systems, the potential impact of dust contamination on these data needs to be evaluated. Furthermore, high-spectral resolution instruments such as the Atmospheric InfraRed Sounder (AIRS) launched recently on the NASA AQUA satellite and the Infrared Atmospheric Sounding Interferometer (IASI) to be launched on the EUMETSAT operational polar platform, sense over

0148-0227/03/2002JD002571$09.00

the same infrared spectral band as HIRS and may also be subject to dust contamination.Several studies hint of aerosol contamination. (1) Recent global ECMWF reanalysis (ERA-40) showed substantial increase in tropical rainfall rates from the second half of 1991 onward. This was due in part to effects of volcanic aerosols on HIRS infrared radiances following the eruption of Mount Pinatubo. These anomalies did not occur when the model was run in climate-simulation mode. (A. Simmons, personal communication, 2002). (2) *Alpert et al.* [1998] report similar patterns in the monthly mean fields of GEOS-1 [*Schubert et al.*, 1993] assimilation temperature increments and dust over the eastern tropical North Atlantic. Increments in a Data Assimilation System (DAS) are defined as the difference between the analysis and the general circulation model (GCM) short-term forecast terms. They include information about physical processes missing from the GCM used in the assimilation. This spatial correlation has been attributed to the GCM not simulating the aerosol radiative forcing in the real atmosphere. However, in addition to these errors in the GCM temperature, there may also be errors in the temperature observations themselves- the NOAA National Environmental Satellite Data and Information Service (NESDIS) TOVS temperatures retrievals. (3) *Weaver et al.* [2002] report that calculations of outgoing long wave fluxes using assimilated temperatures and moisture values consistently decrease with increased atmospheric dust loading in the Saharan region. Since no information about the dust distribution is used in the radiative calculations, the conclusion was that the dust affects the assimilated temperatures and moisture indirectly. One mechanism is that the NESDIS TOVS temperatures retrievals, which are used as observations in the assimilation, are systematically colder during heavy dust loading conditions. These colder temperatures yield reduced outgoing longwave radiation. (4) *Diaz et al.* [2001] find that there is a significant increase in the errors of sea surface temperatures (SST) retrieved by the advanced very high resolution radiometer (AVHRR) in the presence of dust aerosols. The Earth Probe Total Ozone Mapping Spectrometer (TOMS) aerosol index (AI) is used to determine the level of aerosol loading. *Nalli and Stowe* [2002] provide an empirical correction algorithm for the AVHRR SST data set by correlating the aerosol optical depth from AVHRR channel 1 (0.63 μm) with the difference between the buoy temperatures and the retrieved SSTs.

2. Gocart Dust Model

[3] All information on the dust spatial and vertical distribution for this study is from the Goddard Ozone Chemistry Aerosol Radiation Transport (GOCART) model. It is an off-line transport model driven by assimilated meteorological fields from the Goddard Earth Observing System Data Assimilation System, GEOS-1 [*Schubert et al.*, 1993]. This model does a good job of simulating dust outbreaks over Africa [*Ginoux et al.*, 2001]. Figure 1 shows optical depths observed by MODIS and simulated by GOCART during early June 2001. Our study will focus on the impact the dust from this event has on the TOVS radiances over the ocean portion of the boxed region in the figure. On 2 June the dust is only observed and simulated just off the African coast; the western portion of the box is clean. By 6 June both GOCART and MODIS show significant loading over the south-west quadrant of the box. The outbreak continues at least until 9 June. *Ginoux et al.* [2001] provides details of the GOCART model and validates it with LIDAR, satellite, and ground-based measurements.

[4] The transport model horizontal resolution is 2.5° longitude x 2.0° latitude. There are a total of 41 vertical sigma levels with 29 levels below 100 mb. The model transports four size ranges from 0.1 to 10 micron using a three-dimensional flux form semi-Lagrangian scheme. The dust source module is based on archived surface wetness, local wind speed, and eddy diffusion. The model accounts for convective and diffusive transport by using archived cloud convective mass flux and vertical eddy diffusion coefficients. Removal by wet deposition requires three-dimensional precipitation information. Since the assimilation only saves precipitation rates at the Earth's surface, information on the vertical precipitation rate is estimated.The model accounts for gravitational settling.

3. TOVS Observations and Radiative Transfer Model

[5] The TOVS consists of three instruments: the High-Resolution Infrared Radiation Sounder-2 (HIRS-2), the Stratospheric Sounding Unit (SSU) and the Microwave Sounding Unit (MSU) [*Smith et al.*, 1979]. Advanced TOVS consists of HIRS-3 which has a different size footprint, and the Advanced Microwave sounding units A and B (AMSU-A and AMSU-B). We focus on HIRS because information on dust spatial distribution and optical properties likely to effect this instrument are available. Dust may also affect the SSU, but we have less information about stratospheric aerosol. The MSU is also susceptible but only the largest dust particles, near the source, will effect the radiances. For example a 5 μm particle at 57 GHz frequency has a size parameter of 0.001 which will cause some Raleigh scattering. Away from the dust source the effect on the microwave is expected to be negligible.

[6] Each channel has a peak energy altitude determined by the vertical profile of constituents that absorb at its bandpass frequencies. Figure 2 shows normalized weighting functions for the HIRS channels. Additional information on each channel is shown in Table 1.

[7] The nighttime monochromatic radiative transfer equation used to calculate the upwelling radiance, I_ν at a frequency v impinging on a satellite is given by

$$I_\nu = \epsilon_\nu \Im_\nu(p_s, 0) B_\nu[T_s] + \int_{ps}^{0} B_\nu[T(p)] \frac{\partial \Im_\nu(p, 0)}{\partial p} dp. \quad (1)$$

[8] The first term represents the contribution from the Earth's surface: p_s is surface pressure, ϵ_ν is the emissivity of the Earth's surface, $\Im_\nu(p_s,0)$ is the transmittance from the surface to the satellite (p = 0) and $B_\nu[T_s]$ is the Planck function at the surface temperature, T_s. The term inside the integral is the contribution of an atmospheric pressure layer (dp), $\Im_\nu(p,0)$ is the transmittance from layer to the satellite, $B_\nu[T(p)]$ is the Planck function at the average temperature of the layer. The weighting functions hown in Figure 2 are related to the $\partial\Im_\nu(p,0)/\partial p$ term.

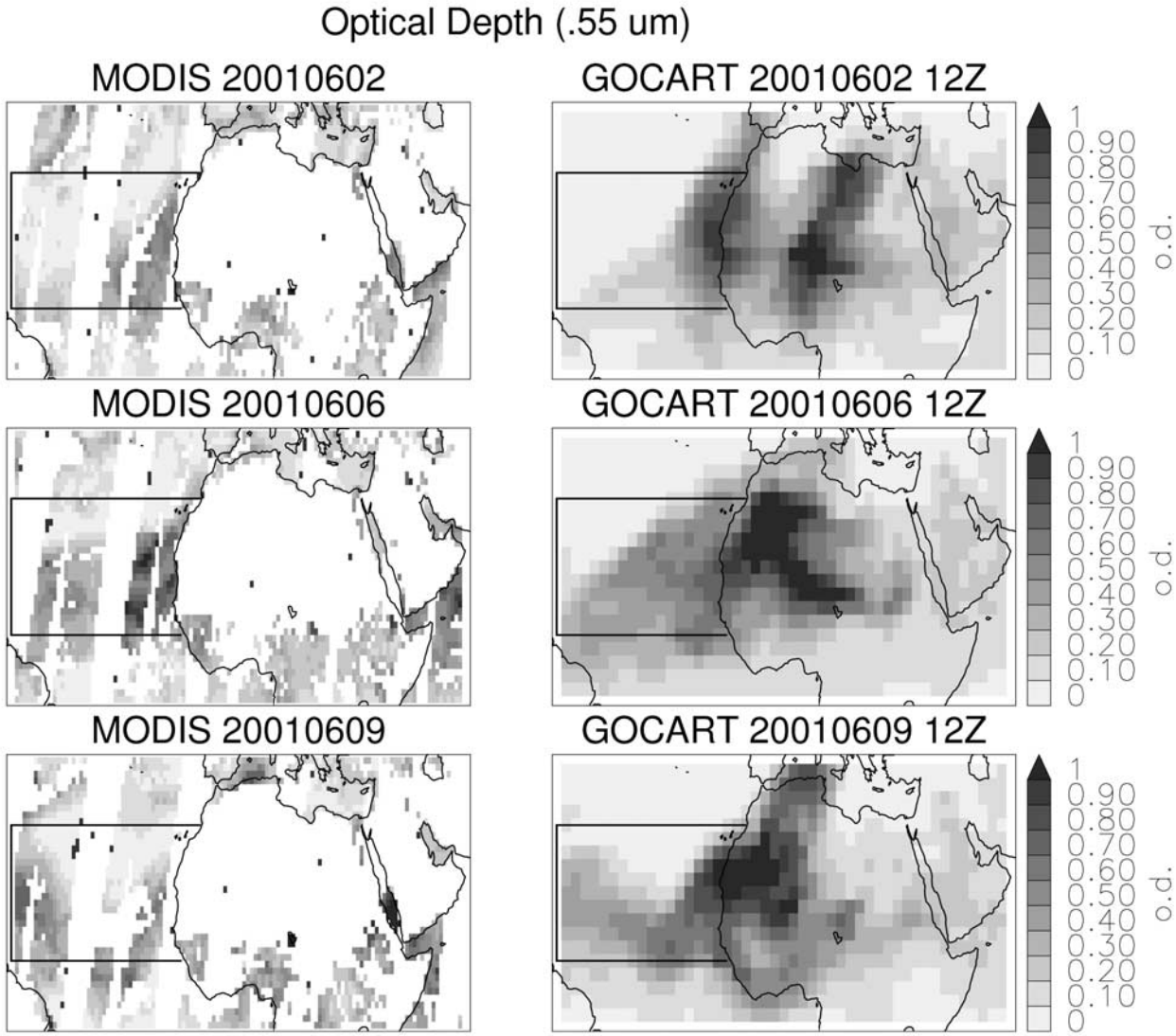

Figure 1. Total column dust loading from GOCART on 2, 6 and 9 June 2001 12Z. There are no MODIS retrievals over North Africa because it is difficult to sense the dust above the bright desert surface in the visible wavelengths.

[9] In fast radiative transfer algorithms, the same equation is used, but transmittances are parameterized for the channel spectral response function. Here we use a fast model called the Goddard Laboratory for Atmospheres TOVS (GLATOVS) developed by *Susskind et al.* [1983]. It includes additional terms such as reflective downwelling thermal radiation and IR solar source terms not shown in equation (1). Comparison of brightness temperatures computed by the fast model with those from a line-by-line models show errors below 0.1 K for the temperature sensing channels and a bit larger for the moisture channels, [*Susskind et al.*, 1983]. It is convenient to convert the radiances to an equivalent black body brightness temperature, T_b. The Planck function of this temperature is the upwelling radiance, I_ν, i.e., $I_\nu = B_\nu[T_b]$. Presence of absorbing dust in the atmosphere reduces the transmittance in both terms of equation (1), which changes the brightness temperature. The aerosol transmittance for a given frequency is approximated by $\Im = e^{-\tau(1-0.5*\omega)}$ where τ is the total aerosol optical depth and ω is the single scattering albedo. The total aerosol optical depth is the sum of optical depths for each size bin (n) which is given by:

$$\tau_n = (3/4) * M(n) * Q_{ext}(n)/\left(r_{eff}(n) * \rho(n)\right) \tag{2}$$

The equations used to sum τ and ω are:

$$\tau = \sum_{n=1}^{n=4} \tau_n \tag{3}$$

$$\omega = \frac{\sum_{n=1}^{n=4} \tau_n * \omega_{0n}}{\tau} \tag{4}$$

where M(n) is the column mass of aerosols vertically integrated from the GOCART dust concentrations, Q_{ext} and

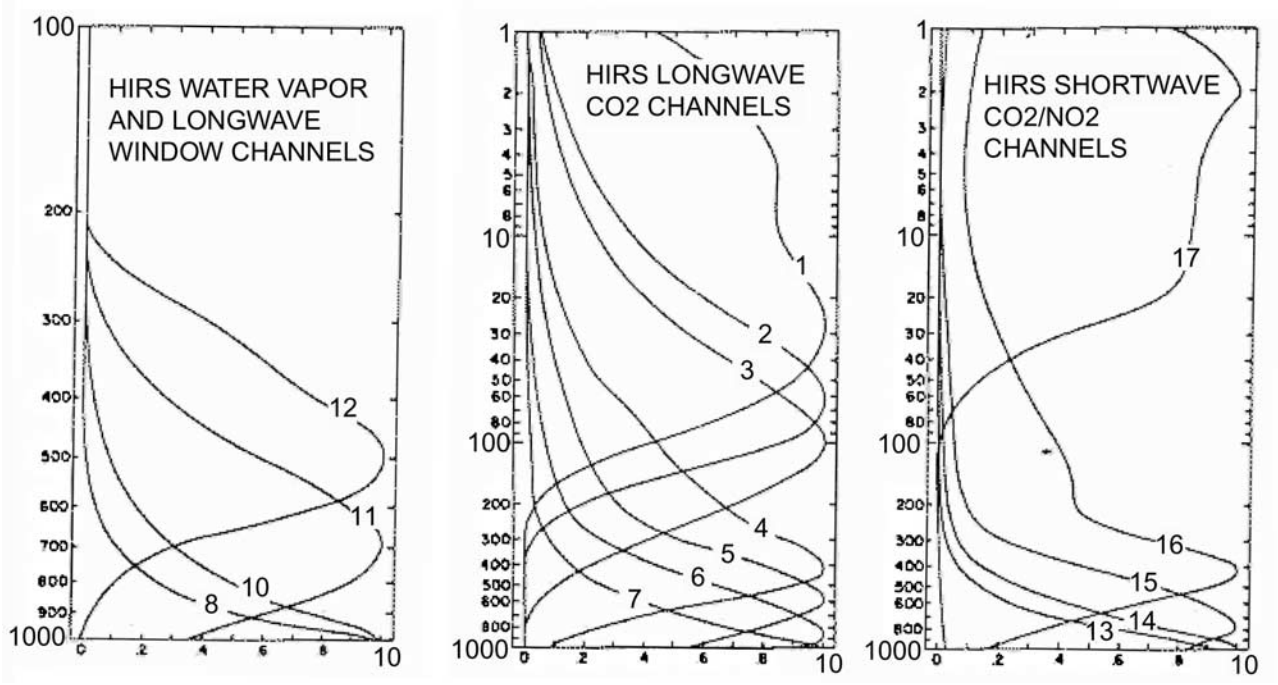

Figure 2. HIRS-TOVS weighting functions (normalized) from *Smith et al.* [1979]. Channel numbers in parentheses.

ω_0 are the extinction efficiencies and single scattering albedoes, r_{eff} and ρ are the effective radius and density of the particles.

[10] Figure 3 shows extinction coefficients and single scattering albedoes for particles composed of either pure illite or hematite for two of the seven GOCART size bins. The illite values are probably more appropriate for dust, since Saharan soil samples usually contain a high fraction of illite [*Sokolik and Toon*, 1999]. All radiative calculations for this study will use the illite optical parameters. Hematite is shown here because it is a strong absorber in the infrared. For illite channels 9 (9.6 μm) and 13–19 (4 μm) have higher extinction efficiencies than the other channels.

4. Brightness Temperature Sensitivity

[11] The sensitivity in the brightness temperature to the dust concentration at a given level is the Jacobian $\partial T_{b_i}/\partial \chi_j$, where T_{b_i} is the brightness temperature of channel i and χ_j = GOCART dust concentration ($\mu g/m^3$) at level j. To compute the sensitivity of a clean (dust-free) atmosphere, vertical profiles of temperature, moisture, ozone and underlying surface temperature were input to the GLATOVS radiative

Table 1. Characteristics of HIRS Sounding Channels, Adapted From *Smith et al.* [1979]

HIRS Channel Number	Central Wavelength, μm	Principal Absorbing Constituents	Level of Peak Energy Contribution	Primary Use
1	15.00	CO_2	30 hPa	temperature sounding
2	14.70	CO_2	60 hPa	temperature sounding
3	14.50	CO_2	100 hPa	temperature sounding
4	14.20	CO_2	400 hPa	temperature sounding
5	14.00	CO_2	600 hPa	temperature sounding
6	13.70	CO_2/H_2O	800 hPa	temperature sounding
7	13.40	CO_2/H_2O	900 hPa	temperature sounding
8	11.10	window	surface	surface temperature
9	9.70	O_3	25 hPa	total column ozone
10	12.56	H_2O	900 hPa	water vapor sounding
11	7.30	H_2O	700 hPa	water vapor sounding
12	6.70	H_2O	500 hPa	water vapor sounding
13	4.57	N_2O	1000 hPa	temperature sounding
14	4.52	N_2O	950 hPa	temperature sounding
15	4.46	CO_2/N_2O	700 hPa	temperature sounding
16	4.40	CO_2/N_2O	400 hPa	not used in DAO-TOVS
17	4.24	CO_2	5 hPa	not used in DAO-TOVS
18	4.00	window	surface	surface temperature
19	3.70	window	surface	surface temperature

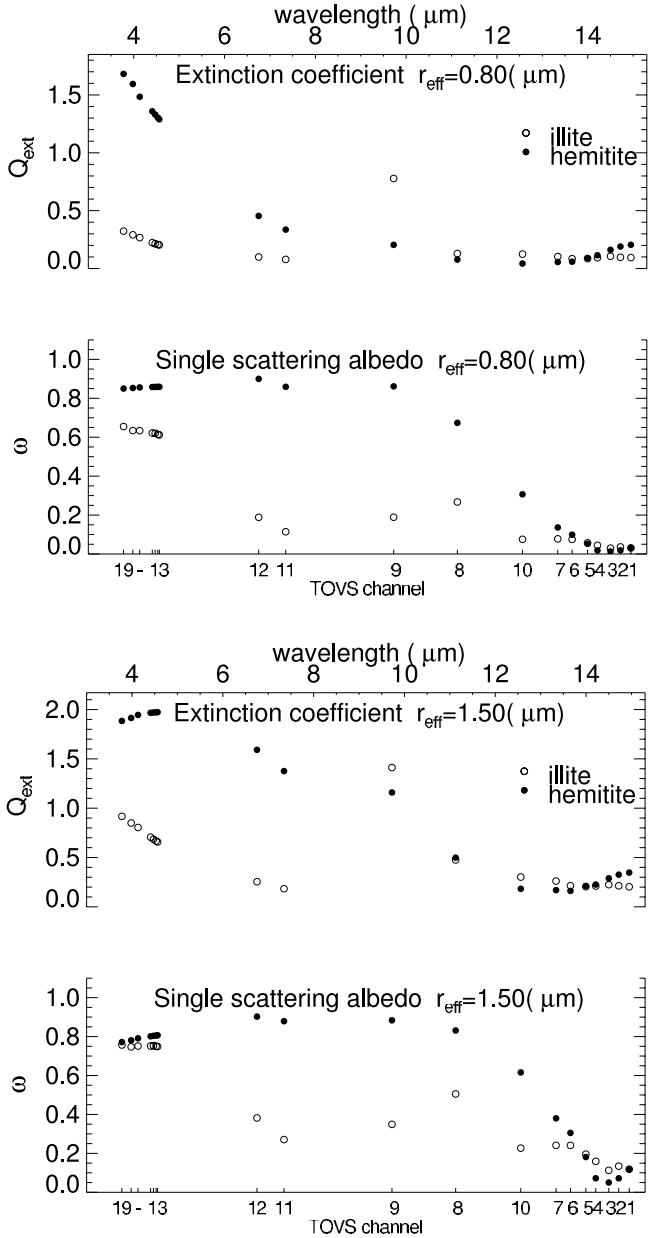

Figure 3. Extinction efficiency (Q_{ext}) and single scattering albedo (ω) at the HIRS frequencies for NOAA-14 assuming particles composed of pure illite and pure hematite. Calculations are done assuming a lognormal distribution with effective radius (r_{eff}) of 0.8 and 1.5 μm and an effective variance of 0.2.

transfer model. We used a representative number of profiles from the first guess assimilated data over ocean just off the coast of Africa. One calculation was performed assuming clean conditions, T_b^{clean}. A second set of calculations was performed by adding a tiny amount of dust to the clean profile at each vertical level and each particle size bin, T_b^{dust}.The Jacobian is computed by finite differencing, i.e., $\partial T_{b_i}/\partial \chi_i = (T_{b_i}^{dust} - T_{b_i}^{clean})/\chi_j$.

[12] Figure 4 shows the $\partial T_{b_i}/\partial \chi_i$ near 800 mb. The channel most sensitive to the total column ozone (HIRS-9) has the highest extinction coefficients and is the most sensitive to dust. Those channels that have their peak altitude weighting function at or below the dust layer and have significant extinction coefficients should be and are dust sensitive (e.g., HIRS-7, 8, 10, 13, 14, 18, 19). Except for HIRS-9, the smaller particles between (.1–1.0 μm) are not as effective at changing T_b. The larger particles are more efficient at extinction and changing the brightness temperatures.

[13] Figure 5 shows the altitude dependence of $\partial T_{b_i}/\partial \chi_j$. For all channels and tropospheric altitudes the presence of dust reduces T_b. Addition of dust at a given pressure level reduces the contribution of the atmospheric and surface emission below that pressure level. Since the temperature below the dust is generally warmer than above the dust, the T_b for the perturbed atmosphere will be less than the T_b of the clean. For each channel, T_b sensitivity to dust increases with altitude. Dust located high in the troposphere, where the atmospheric temperature is cold, will contribute to colder brightness temperatures compared with dust radiating at warmer atmospheric temperatures below. The vertical profile of $\partial T_{b_i}/\partial \chi_j$ is consistent with the weighting functions (Figure 2). The atmosphere below 600 hPa contributes little to HIRS-3 whose weighting function peaks near 100 hPa so that the presence of dust in the lower troposphere is not sensed by this channel. However, channels that sense the lower troposphere (e.g., HIRS-8, 11 and 18) have significant $\partial T_{b_i}/\partial \chi_j$ in the lower troposphere. The window channels HIRS-8 and 18 have more sensitivity to dust near the surface than HIRS-11 which is more sensitive to tropospheric humidity and has a weighting function that peaks higher in altitude.

[14] A complicating issue is that the $\partial T_{b_i}/\partial \chi_j$ for channels that sense water vapor (10, 11 and 12) changes with the atmospheric water vapor amount. Figure 6 shows the vertical profiles of $\partial i_{b_i}/\partial \chi_j$ for different atmospheric water vapor amounts. The solid lines show the profiles when the full value of the first guess moisture is used in the radiative transfer calculation. The dotted and dashed show profiles from calculations that use only a fraction of the first guess moisture values. The channels that have water vapor as their principal absorbing constituent, HIRS-10 (not shown) and HIRS-11 and 12 are significantly more sensitive to dust under dry compared with moist conditions. HIRS-6 and 7 (not shown) which also absorb water vapor have a small moisture dependence. All the remaining channels (HIRS-1 through HIRS-5, 8, 9 and HIRS-13 through HIRS-19) show negligible moisture dependence on the $\partial T_{b_i}/\partial \chi_i$.

[15] Note that illite was assumed for these calculations. The actual dust being sensed by TOVS in this region may have a different composition and spectral signature. For example, our calculated sensitivity would be much larger at channel 11 and 12 if the dust had a hematite coating.

[16] For Figures 4, 5, and 6, the Jacobian was calculated by perturbing a clean profile. Jacobians calculated by perturbing a typical dust profile (not shown) have the same qualitative characteristics as those shown.

5. The fvDAS Results

[17] The Finite-Volume Data Assimilation System (fvDAS) from the Data Assimilation Office (DAO) uses a new finite-volume dynamical core (fvGCM) model and the NCAR physical parameterizations Community Climate

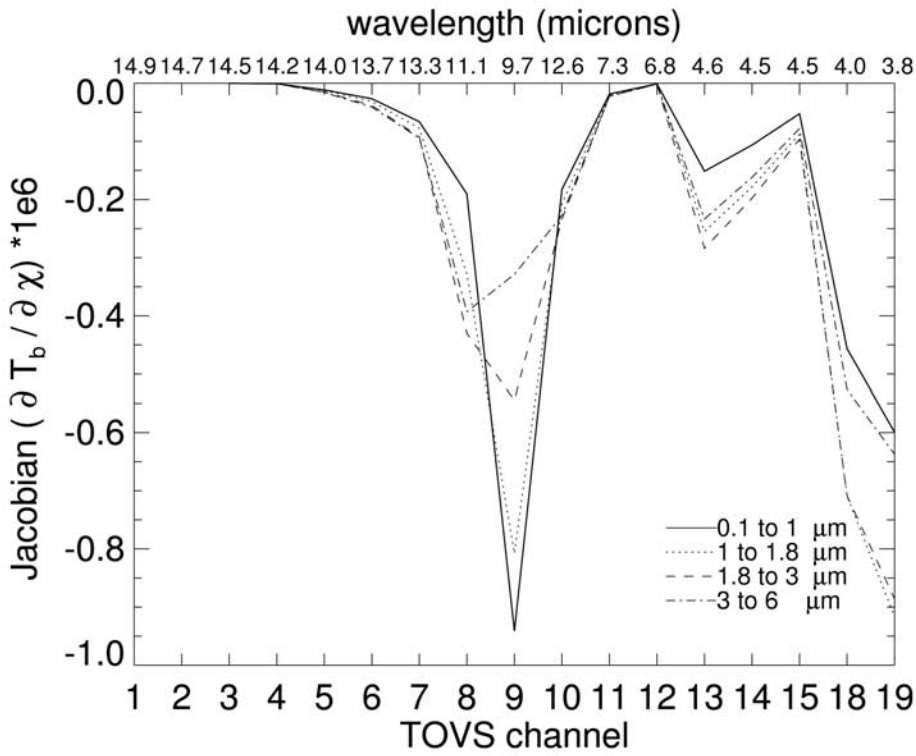

Figure 4. Sensitivity ($\partial T_{b_i}/\partial \chi_j$) * 1e6 K/(μg/$m^3$) of brightness temperature to dust loading for the four transported GOCART size bins. The difference in brightness temperature between a dust-free atmosphere over tropical ocean and one perturbed by adding a small amount of illite at 792mb is used in the calculation of $\partial T_{b_i}/\partial \chi_j$. Sensitivities are shown for the NOAA-14 HIRS frequencies.

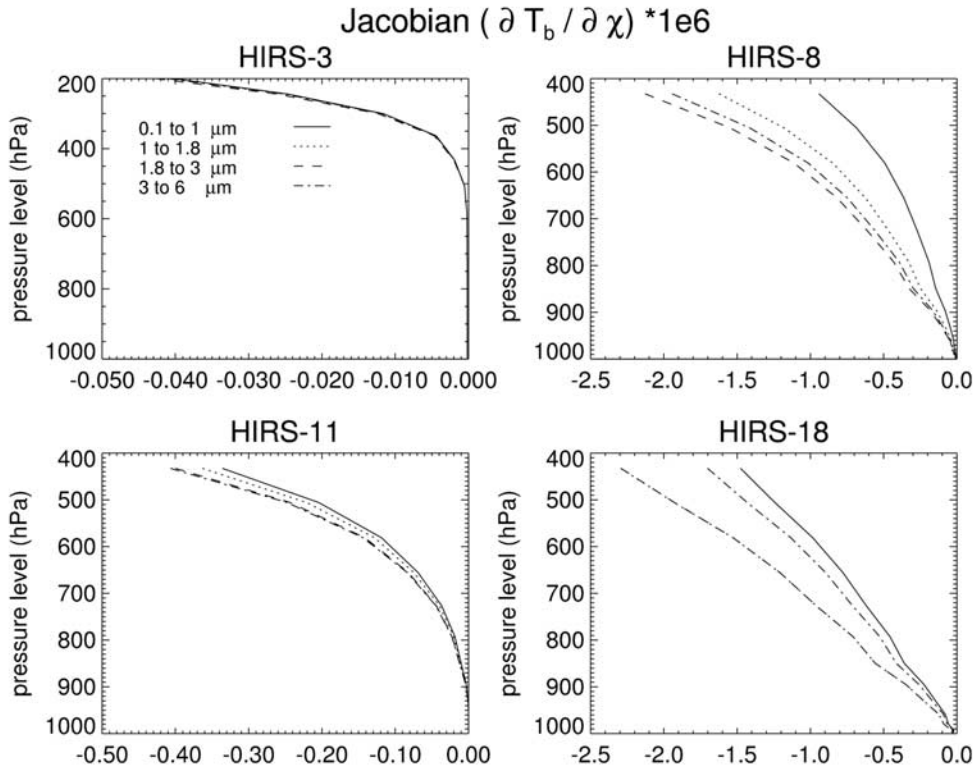

Figure 5. Similar to Figure 4, but showing the pressure dependence of ($\partial T_{b_i}/\partial \chi_j$) for HIRS-3, 8, 11 and 18. For HIRS-18 the 1–1.8 and 1.8–3 μm bins are on top of each other.

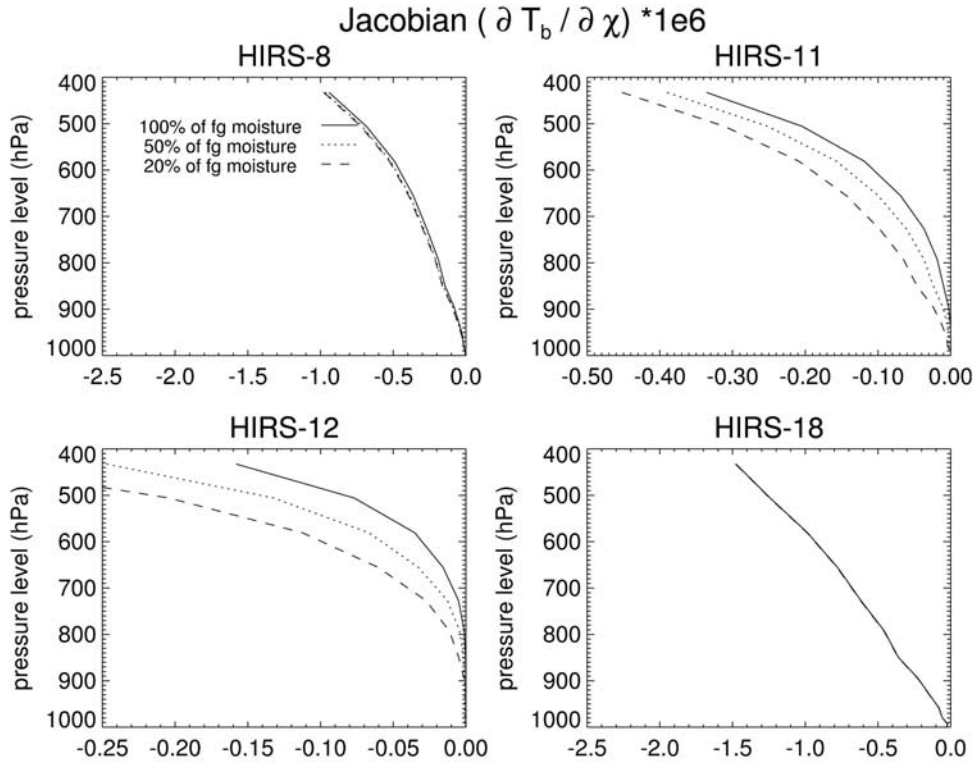

Figure 6. Sensitivity ($\partial T_{b_i}/\partial \chi_j$) of brightness temperature to dust loading for the smallest size bin transported in GOCART (.1–1um). Sensitivities are shown for different water vapor amounts. Solid: the value of the first-guess (background) water vapor amount from the fvDAS assimilation. Dotted: 50% of the first-guess water vapor. Dashed: 20% of the first-guess water vapor.

Model-3 (CCM3) package [*Kiehl et al.*, 1996]. The fvGCM has horizontal discretization built upon the Flux-Form Semi-Lagrangian (FFSL) transport algorithms [*Lin and Rood*, 1996, 1997]. The vertical structure is based on the Lagrangian control-volume concept of *Lin* [1997] and *Lin and Rood* [1998]. This physically-based dynamical core circumvents many of the problems associated with sigma, pressure, or isentropic coordinates, increasing the physical integrity and computational efficiency of the model.

[18] Starting with the initial fields the fvGCM is run forward for 6 hours. The modeled temperature and moisture profiles are used as a first guess in the interactive cloud-clearing TOVS (DAO-TOVS) retrieval system of *Joiner and Rokke* [2000]. This retrieval system attempts to remove the radiative effects of clouds by comparing partly cloudy adjacent pixels. The resulting cloud-cleared brightness temperatures are those estimated for clear sky conditions. However in dusty conditions, DAO-TOVS may be clearing the effects of dust instead of clouds. Since its difficult to separate the effects of dust and clouds, we do not consider any DAO-TOVS scenes where cloud-clearing occurred. A diagnostic of DAO-TOVS is the observed minus forecast residuals of brightness temperature (O–F). The retrieved and first guess temperatures along with other observational data (e.g., radiosondes and other conventional data, scatterometer winds, SSMI total precipitable water) are presented along with the 6 hour forecast to the Physical-Space Statistical Analysis System (PSAS) [*Cohn et al.*, 1998] which computes increments in the height, moisture and wind fields that are used as initial conditions for the next fvGCM forecast.

[19] Presently, the standard DAO fvDAS does not account for dust in either the retrieval algorithm or in the calculation of the heating rates. We ran 14 days of the standard fvDAS starting on 2 June 2001. If dust is contaminating the DAO-TOVS retrievals we would expect to find smaller residuals in the O–F brightness temperatures under pristine conditions and larger residuals when there is heavy dust loading. However, there are many other factors besides dust that influence O–F brightness temperatures. For example biases in O–F can be due to (1) errors in the fvGCM which provided the first guess temperatures and moisture profiles, (2) incorrect assumptions used in the radiative transfer model that calculated the brightness temperatures, (3) errors in the observations themselves.

[20] In order to avoid the solar contribution to the O–F brightness temperatures for the solar affected IR channels, HIRS-18 and 19, we restrict our analysis to night time observations. During the day the surface bi-directional reflectance for these channels is not precisely known which leads to large biases for these channels. At night the surface IR emissivity is modeled accurately over ocean using the model of *Masuda et al.* [1988] and the biases are relatively small. Another issue is that the IR surface emissivity and skin temperature over land are not well known and this

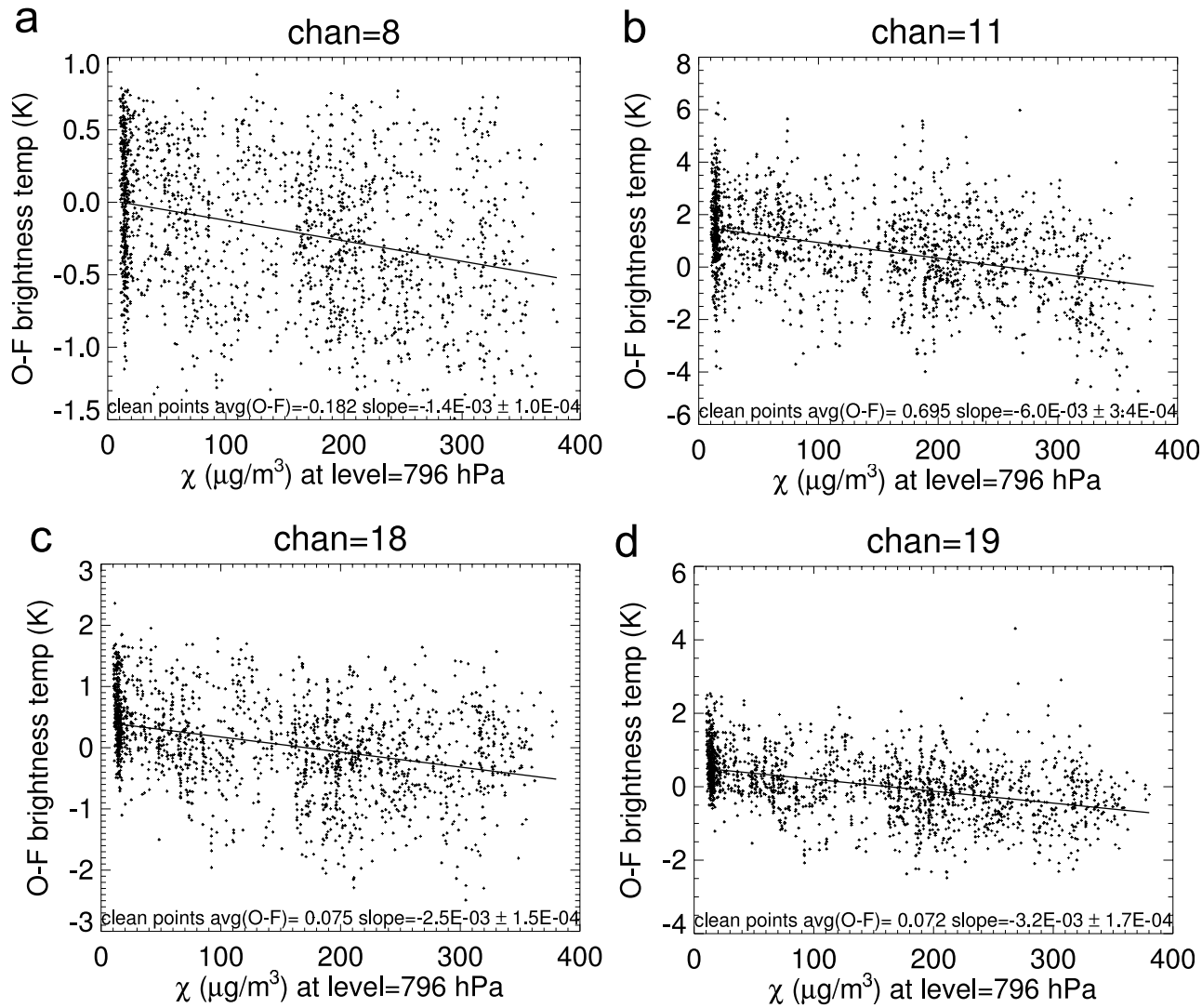

Figure 7. (a–d) Each point is the observed minus forecast T_b^{clean} from an fvDAS standard run plotted against the collocated amount of dust in GOCART. Observations are from NOAA-14 sounded between 2–11 June 2001 at 3am local time. Only cloud-free pixels over ocean are shown. The average O–F brightness temperature and the best-fit slope and its uncertainty are also shown.

leads to larger biases than over ocean. Therefore we restrict our analysis to night time retrievals over ocean.

[21] The DAOTOVS includes a bias correction to the brightness temperatures based on available radiosondes. While this draws the global average of O–F toward zero, individual locations may experience large biases due to errors in sea surface temperature (SST) in addition to the above-mentioned sources of error. The SSTs used in the fvGCM are from a weekly bulk surface temperature analysis that used AVHRR retrievals [*Reynolds and Smith*, 1994]. However, the infrared channels are sensitive to the skin temperature which varies on diurnal and daily timescales. Furthermore, The AVHRR retrievals are also subject to errors from dust contamination. During a Saharan dust outbreak in situ buoy SST minus satellite derived SST can be on the order of 1K [*Diaz et al.*, 2001; *Nalli and Stowe*, 2002].

[22] To determine the level of dust loading in the atmosphere we could use satellite imagery (e.g., the TOMS aerosol index or AVHRR), but this provides no information about the vertical structure of the dust, nor would it provide sufficient information about the particle size. Instead we use dust concentrations from a GOCART model, run with assimilated winds during the period of interest. About a week after we initialize the fvDAS there was a strong dust outbreak over Africa (Figure 1).

[23] Figure 7 shows HIRS-8, 11, 18 and 19 O–F brightness temperatures from all the cloud-free scenes over ocean during the 2-week fvDAS run. To be declared cloud-free, the radiances are subjected to a number of checks [*Joiner and Rokke*, 2000] including a restrictive background test that $|O-F|\ T_b$ for HIRS-8 < 1.5 K. The residual from each observation is plotted against the simulated GOCART dust concentration at the time and location of the observation. Even though there is no dust information from GOCART (or any aerosol satellite data) used in this assimilation run, there is a clear dependence between O–F T_b^{clean} and dust loading in the GOCART model. The forecasted brightness temperatures are consistently colder than the observations under heavy

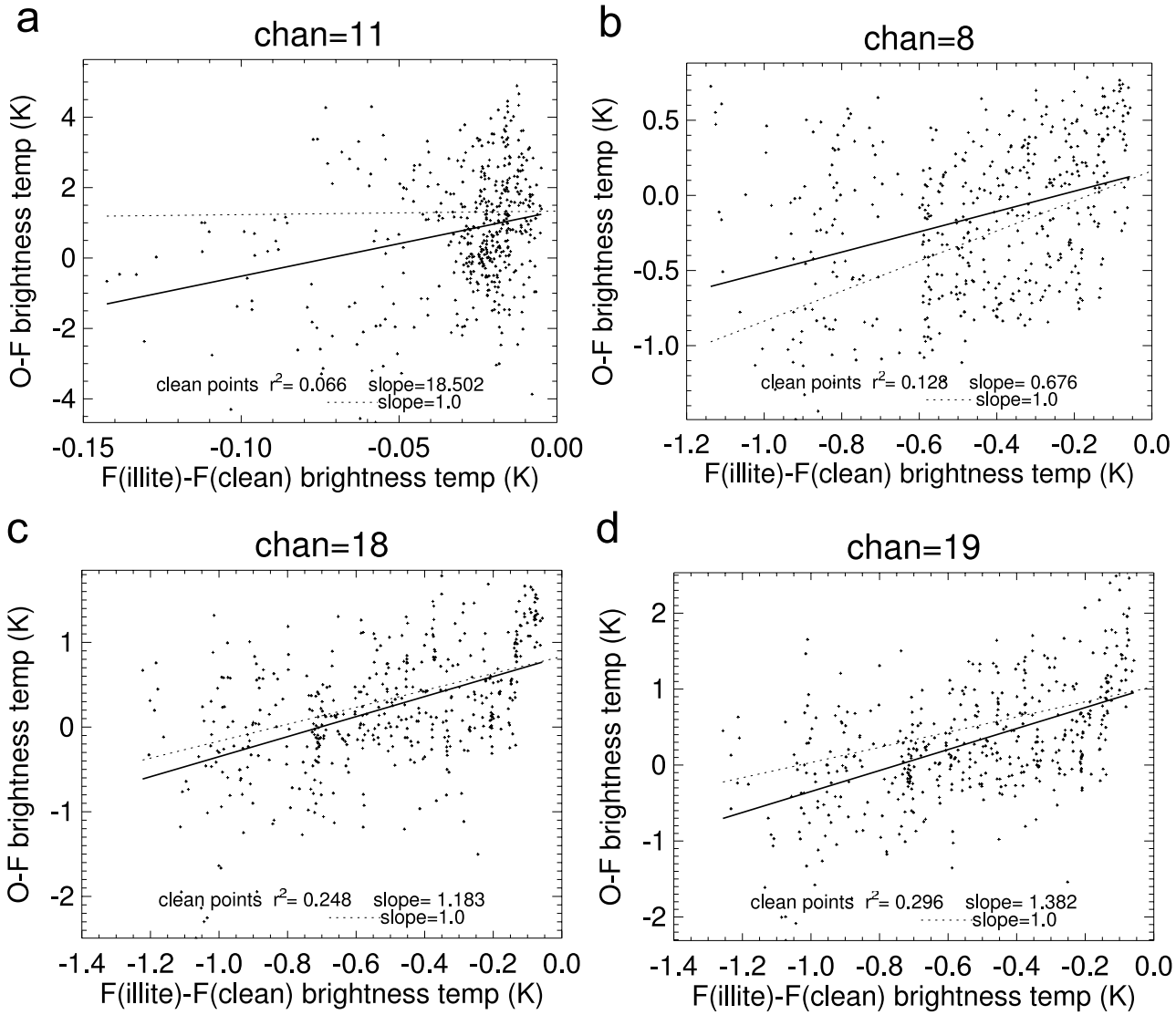

Figure 8. (a–d) Each point is the observed minus forecast T_b^{clean} for a DAO-TOVS retrieval from an fvDAS standard run plotted against the expected change in brightness temperature from illite absorption. This temperature difference is the forecast T_b assuming GOCART dust concentrations and illite optical properties F(illite) minus the forecast T_b assuming a clean atmosphere, F(clean). See text. Linear regression lines are solid and dotted lines have a slope of unity.

dust loading conditions. Even though the points are widely scattered, the range of slope values within the slope uncertainty is always negative. HIRS-18 shows a 1 K residual in the brightness temperature under the heaviest loading conditions. Other channels that are sensitive to the surface temperature (HIRS-8 and 19) also show a significant change in brightness temperature in the presence of dust. The most sensitive channels are the water vapor channels (HIRS-11 and 12, shown later in Figure 9) with up to a 4 K O–F residual.

[24] To understand this dependence we can calculate the difference in the brightness temperature, based on the temperature and moisture profiles of each scene, with and without the GOCART dust, and assume the dust optical parameters are from pure illite. Refractive indices in the infrared are taken from *Querry* [1987]. These brightness temperature differences are plotted against O–F T_b^{clean} in Figure 8. Because both ordinates of Figure 8 are in units of brightness temperature, a slope of one indicates that GOCART dust particles composed of illite provide the right amount of extinction to explain the O–F T_b^{clean} from the fvDAS assimilation. HIRS-8, 18 and 19 are reasonable but our model is clearly not adequate for HIRS-11.

[25] One explanation is that the value for the extinction efficiency derived from the indices of refraction of illite is too small for HIRS-11. Hematite has the highest extinction of any of the minerals that might make up the dust particles. Although its unlikely that the dust is composed of pure hematite, there may be an outside coating. However, even if a hematite coating is assumed, the differences in brightness temperature with and without GOCART dust fail to explain the 3 K O–F T_b^{clean} values seen in Figure 8. Another more subtle explanation is that increasing $\partial T_{b_i}/\partial \chi_j$ with decreasing water vapor (Figure 6) combined with the a bias in the first guess water vapor values (D. Dee, personal communi-

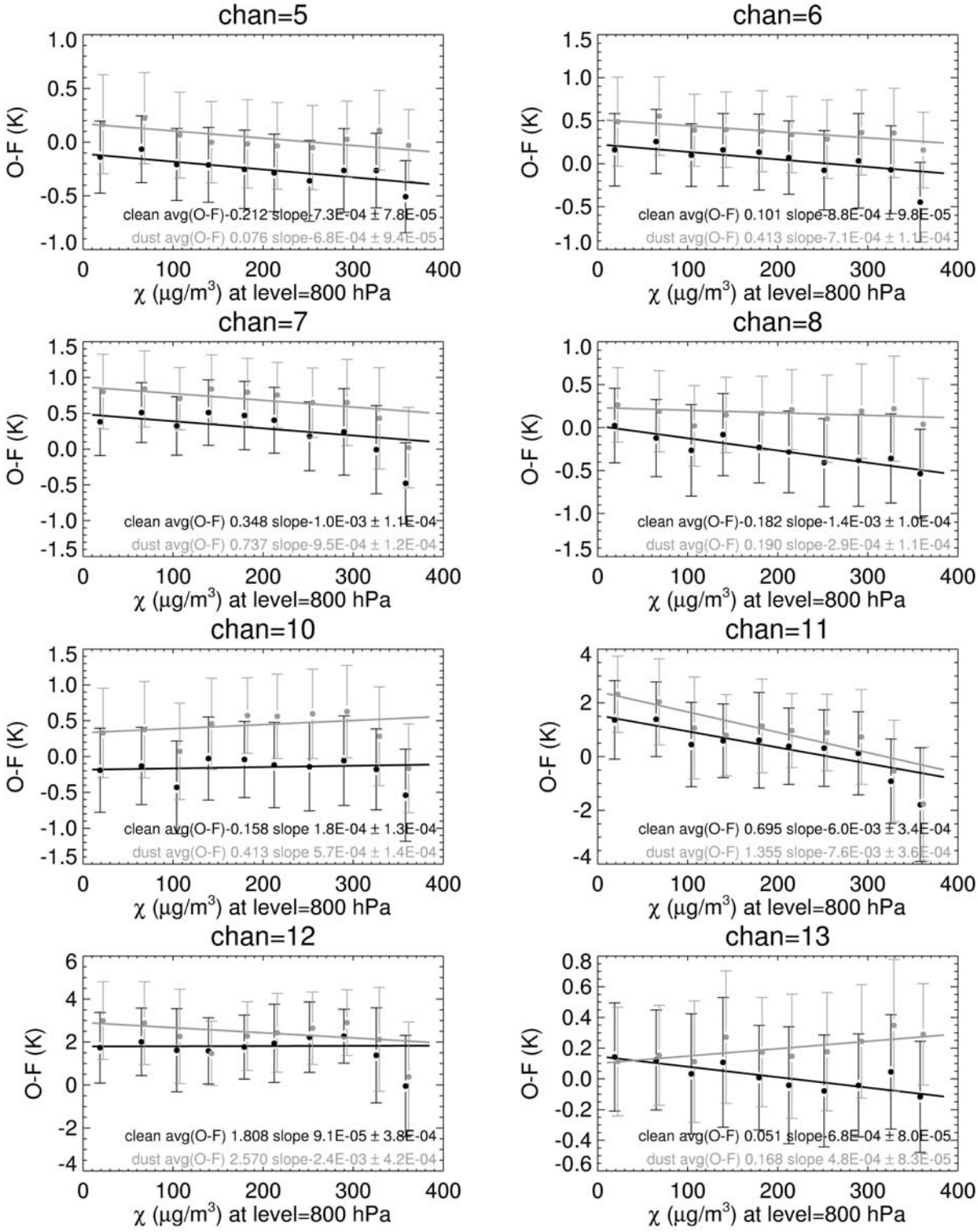

Figure 9. Observed minus forecast brightness temperatures vs. the dust concentration in the GOCART model at 800 hPa. Black points (T_b^{clean}) are from a standard fvDAS run with an DAO-TOVS package that does not account for dust. Grey points (T_b^{dust}) are from a special run with an DAO-TOVS package that assumes GOCART dust concentrations and optical parameters of illite. Each point is an average of O−F brightness temperatures from many pixels that fall between a given dust concentration interval. Observations are from NOAA-14 sounded between 2−11 June 2001 at 3am local time and from only cloud-free conditions over ocean.

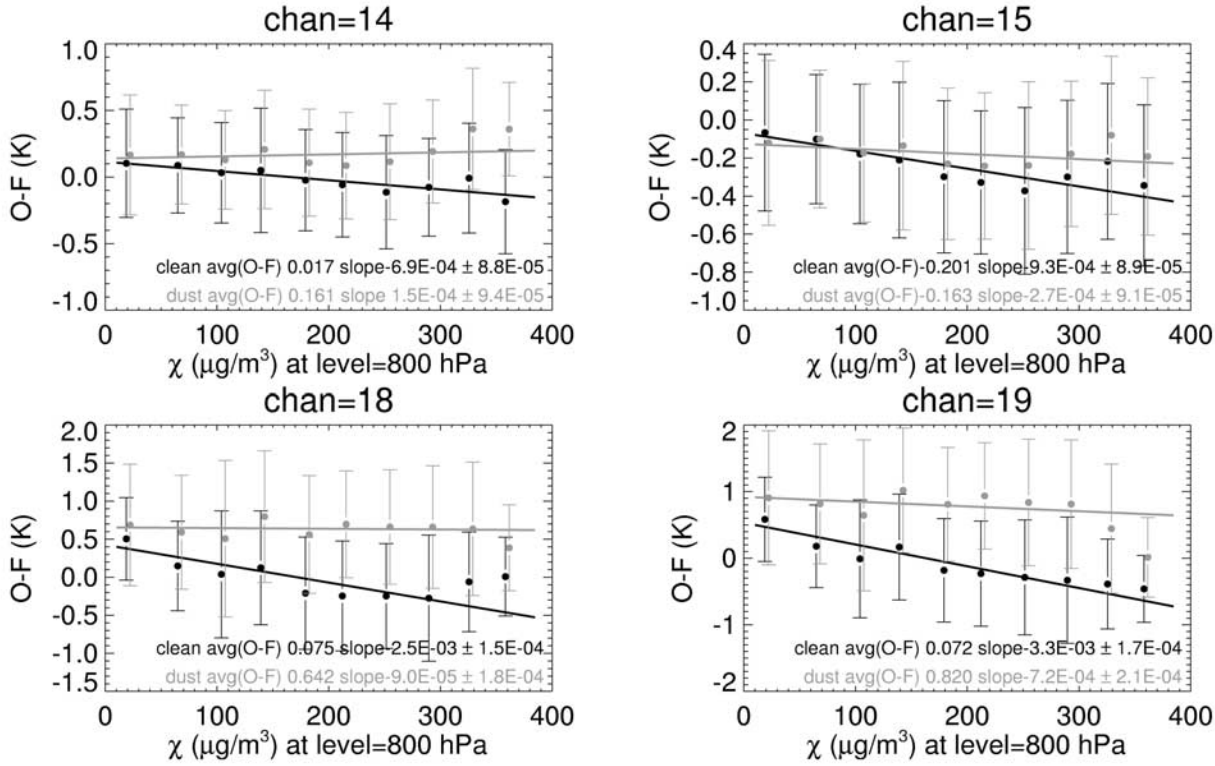

Figure 9. (continued)

cation, 2002), could lead to large changes in T_b^{clean}. However, calculations (not shown) that assume a totally dry atmosphere, and make T_b^{clean} very sensitive to dust, still cannot explain the 3–4 K O–F T_b^{clean} values. A third explanation is a moisture bias that depends on dust loading.

6. Modified fvDAS Results Accounting for Dust Absorption

[26] Since the GOCART dust composed of illite seems to explain the O–F T_b^{clean} bias at least in the temperature-sensing HIRS channels, the radiative transfer model used in DAO-TOVS was modified to account for GOCART dust. We repeated the 14 day fvDAS run starting on 2 June 2001 but used the modified DAO-TOVS package. Figure 9 shows O–F brightness temperatures from this run, T_b^{dust} as well as the standard run (no accounting for dust in DAO-TOVS), T_b^{clean}. Although the swarm of individual pixels (Figure 7) was used to calculate the solid trend lines, they are represented by bin-averaged brightness temperatures (solid circles). The vertical bars are 1 standard deviation of the points used to calculate the average.

[27] The first panel of Figure 9 shows results from HIRS-5. Although it senses temperature via CO_2 absorption in the upper troposphere, there is some contribution lower in the atmosphere near 800 hPa. This might explain the small dependence T_b^{clean} (black points) has with dust loading lower in the atmosphere. Accounting for dust in the DAO-TOVS does not remove this dust loading dependence. In fact the O–F T_b^{dust} bias (grey points) is larger than the T_b^{clean} points. HIRS-6 and 7 sense temperature via CO_2 absorption in the lower troposphere and show a more pronounced dependence between O–F T_b^{clean} and dust loading. Under heavy dust loading conditions the brightness temperatures can be lowered by 0.5 K. HIRS-8 which senses the ground temperature, clearly shows the influence of dust on T_b^{clean}. Accounting for dust in DAO-TOVS yields T_b^{dust} that shows no dependence on dust loading. This is good example where the O–F T_b^{clean} points can be explained by the GOCART model and illite optical parameters (slope near unity in Figure 8), and where accounting for dust in DAO-TOVS yields O–F brightness temperatures that are not influenced by dust loading. HIRS-10 and 12 which, sense water vapor in the troposphere, are complicated by the strong influence of water vapor on $\partial T_{b_i}/\partial \chi_j$. HIRS-10 and 12 show little influence of dust on T_b^{clean} but HIRS-11 shows a pronounced influence. HIRS-13 and 15 are sensitive to N_2O and or CO_2 absorption in the lower troposphere. These channels shows a small influence of dust on T_b^{clean}. Accounting for dust in the DAO-TOVS appears to overcorrect for the presence of dust in HIRS-13, but HIRS-14 and 15 show the desired correction. HIRS-18 and 19 are like HIRS-8 which are primarily sensitive to the surface skin temperature and show a strong dust dependence which can be removed with the modified DAO-TOVS package. HIRS-9 which senses total column ozone is not considered here because of inaccurate background ozone concentrations used in the DAO-TOVS. These errors contribute to large O–F T_b values which are significantly larger than the T_b signal due to dust. Ideally, we would like the dust correction to remove any O–F T_b^{dust} dependence with dust concentration for all affected channels. Channels that

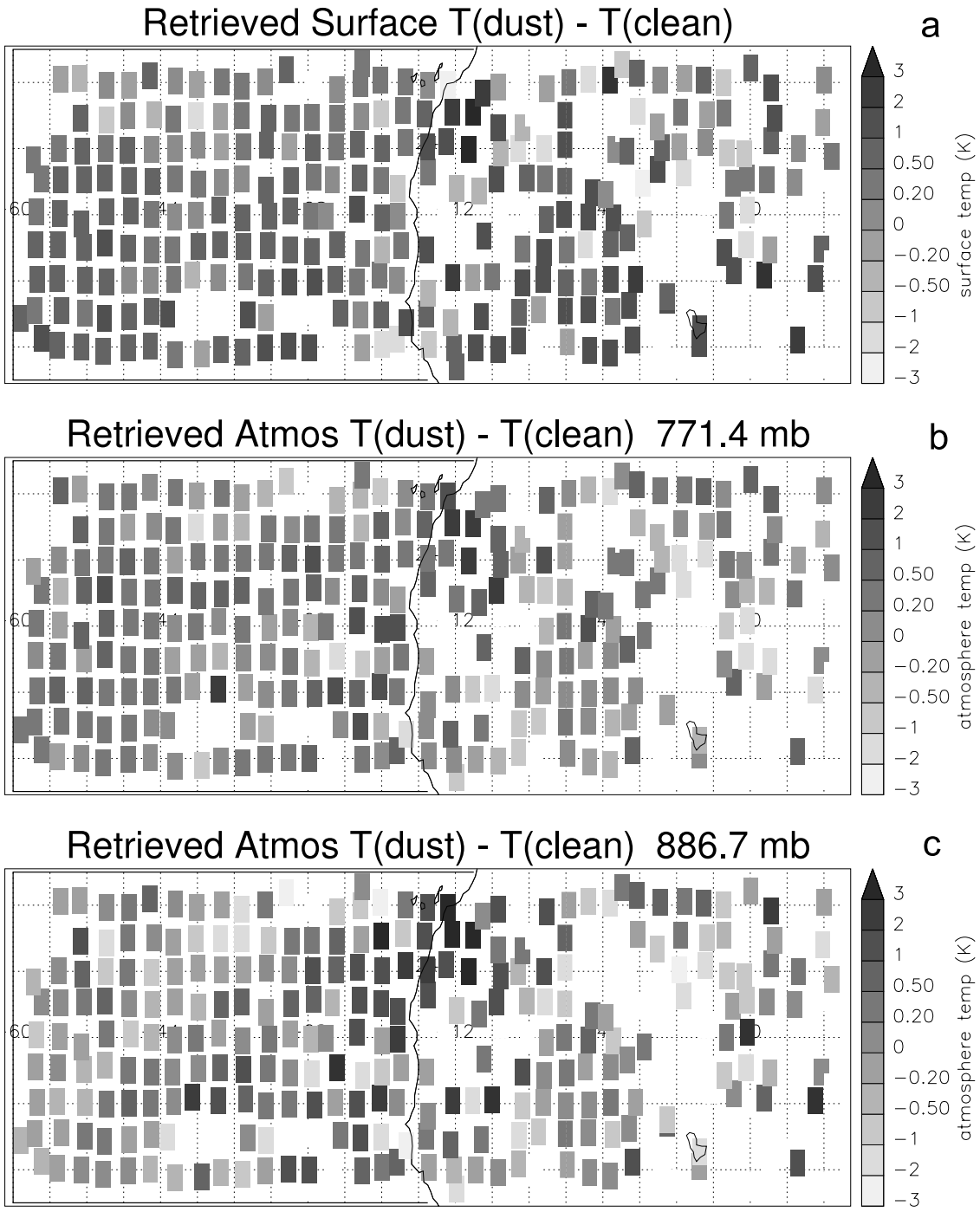

Figure 10. Difference between retrieved temperature from an fvDAS assimilation that accounts for dust minus retrieved temperature from standard assimilation that does not account for dust at (a) surface, (b) 771 hPa, and (c) 886 hPa. Each box represents a time average of temperature retrievals from NOAA-14 sounded from 2–10 June 2001 at 3am local time. See color version of this figure at back of this issue.

show under (e.g., HIRS-5) or over correction (HIRS-13) indicate errors in the assumed optical properties of the dust or errors in the modeled dust vertical distribution.

7. Differences in Retrieved Temperatures

[28] Accounting for dust absorption in the DAO-TOVS changes the retrieved surface and atmospheric temperature fields. Figure 10 shows these differences for cloud-free scenes at the surface and in the lower troposphere. Table 2 shows differences averaged over the tropical Atlantic just off the African coast. Surface temperatures are warmer on average by +0.4K over the tropical Atlantic. In most ocean locations the change is positive which is consistent with $T_b^{dust} > T_b^{clean}$ for the window channels. We have confidence that the retrieved surface temperatures over ocean from the

Table 2. Mean Difference Between Retrieved Temperature From an fvDAS Assimilation With a DAO-TOVS Algorithm That Accounts for Dust Minus Retrieved Temperature From a Standard Assimilation That Does Not Account for Dust[a]

Pressure Level	Temperature Difference
223	0.13
273	0.04
346	0.01
447	0.05
591	0.11
771	0.36
886	0.10
961	0.01
Surface	0.43

[a]Temperatures are averaged from 2–10 June 2001 over ocean between 10–30°N latitude east of 60°W longitude.

modified run are an improvement over the standard run because the window channels, HIRS-8, 18 and 19 show no sensitivity to dust when dust absorption is included in the DAO-TOVS radiative transfer model (grey points of Figure 9). Including dust absorption in the DAO-TOVS yields large increases (>1.0K) in surface temperature over land in some locations.

[29] In the mid to lower troposphere over ocean inclusion of dust in DAO-TOVS warms the atmosphere several tenths of a degree on average (see Table 2). The altitude of the peak atmospheric temperature correction at 771 hPa is qualitatively consistent with the an increasing $\partial T_b/\partial \chi$ with altitude (Figure 5) and a typical dust profile (not shown) which has high concentrations in the lower troposphere and low values above. At the lowest layer in the troposphere the $\partial T_b/\partial \chi$ is small; higher up where the dust concentration is still significant the $\partial T_b/\partial \chi$ is larger, leading to larger brightness and retrieval temperature corrections. In the upper troposphere the dust concentrations are so small that the correction is reduced.

[30] For certain locations in Figure 10, dust can either warm or cool the atmosphere significantly (887 hPa near the African coast). Channels that sense this region of the atmosphere, HIRS-14 and 15, are corrected (grey line of Figure 9 is flat compared to black line) but HIRS 13 is not properly corrected. There also are significant changes in moisture, but the poor corrections to the water vapor sensing channels (HIRS-10, 11 and 12) gives us little confidence in the moisture fields of the modified fvDAS run.

8. Discussion

[31] Non-zero values of O–F T_b arise from errors in either the observations, the radiative transfer model or the forecast model. We have demonstrated a clear dust signal in O–F T_b based on dust information from the GOCART model. However, the mean bias for a given channel is sometimes significantly greater for O–F T_b^{dust} compared with T_b^{clean} (e.g., HIRS-5, 6 and 7). The average O–F values are shown in each panel of Figure 9. Ideally, the mean O–F T_b should be zero when there is no dust and should move closer to zero when dust is included in DAO-TOVS. A procedure to control the mean biases, at least globally, is the tuning of the radiances to collocated radiosondes which is done prior to the actual TOVS retrieval. Coefficients of predictors that include parameters in the radiative transfer model [*Joiner*, 1997] are adjusted based on the radiosondes. A single global coefficient is estimated for each predictor. The predictors are chosen to reduce latitude- and scan-angle-dependent biases. This reduces the global mean O–F T_b. However local biases in O–F remain. The source of these biases include errors in the radiative transfer algorithm and imperfect tuning to remove these biases as well as biases in the first guess temperatures, humidities, and input weekly SST analysis. The tuning procedure for both the modified (T_b^{dust}) and standard (T_b^{clean}) fvDAS run are identical; neither accounts for dust. Accounting for dust in the tuning procedure should not significantly reduce the O–F residuals because there are only a few radiosonde stations in locations of heavy dust loading.

[32] We have shown that inclusion of dust absorption in a TOVS retrieval scheme can significantly change the observed surface temperature and to a lesser extent the atmospheric temperature. Since there are no radiosondes or reliable measurements of skin temperatures over the tropical Atlantic we can not demonstrate improved accuracy, only sensitivity. Still these results will impact any satellite retrieval in the infrared spectrum in the presence of dust.

[33] We could have evaluated the effect of dust absorption by simply running the DAO-TOVS retrieval module with and without dust absorption using identical first guess temperatures. Instead, we ran the DAO-TOVS retrieval within the fvDAS assimilation. This allows any improvements (or degradations) in the retrieved temperature to influence the first guess temperature used in the next retrieval cycle.

[34] We discussed two examples where not accounting for dust absorption could introduce errors in retrieved quantities (1) The AVHRR instrument senses the sea surface temperature by measuring radiation in the 3.5–4.0 μm and 10–12 μm channels. Since these AVHRR channels are close to HIRS-8, 18 and 19 frequencies, the error in the retrieved SSTs are probably the same order of magnitude as the surface temperature differences in Figure 10. *Diaz et al.* [2001] report an association between errors in the AVHRR SST retrievals and aerosol loading determined by TOMS AI. Average errors range from 0.34°C for AI values between 0.5 and 1.0 to 1.74°C for AI greater than or equal to 1.5. These are consistent with our Figure 10. These SSTs have a wide usage including the DAO-fvGCM and most numerical weather prediction systems. *May et al.* [1992] developed a correction algorithm derived from the NOAA AVHRR SST product, optical depth measurements, and from drifting buoy in situ SSTs. (2) The Atmospheric InfraRed Sounder (AIRS) [*Aumann and Pagano*, 1994] was launched in May 2002 on NASA's Earth Observing System (EOS) Aqua platform. It is a high spectral resolution instrument ($\delta\nu/\nu$ = 1200) with 2378 channels from approximately 600 cm-1 to 2700 cm-1 (3.7 to 16.6 μm), designed to measure temperature, humidity and

ozone profiles as well as surface parameters with greater vertical resolution as compared with HIRS. In addition, retrievals of several trace-gas species are proposed, including CO and CO_2. Since AIRS covers the same frequency range sampled by HIRS, except at a higher spectral resolution, many of the retrieved quantities will be susceptible to dust contamination.

[35] Our results are consistent with results of *Weaver et al.* [2002]. Their calculated broadband outgoing longwave radiation (OLR) fluxes consistently showed reduced values in locations of dust loading compared with clean conditions. One would expect that in the real atmosphere the OLR values would be reduced in regions of heavy dust loading. However, these calculations used no GOCART dust information, only temperature and moisture profiles from the Goddard Earth Observing System-2 (GEOS-2) assimilation system were included. The observed temperature used in the GEOS-2 were not interactively retrieved using DAO-TOVS, instead the NESDIS TOVS retrieved temperature fields were used. *Weaver et al.* [2002] suggested that these temperatures are likely systematically cooler than the true temperature because of dust absorption. These cooler temperatures, when used in the radiative calculations, explain the lower OLR the fluxes that they observed. Indeed, the temperature differences in Figure 10 and Table 2 shows how much the retrieved temperatures may be reduced when there is no account of dust absorption in the algorithm.

[36] The effect of dust absorption on retrieved temperature can complicate studies on dust climate forcing. *Alpert et al.* [1998] attempted to use temperature increments from the GEOS-1 DAS assimilation to get a quantitative measure of the atmospheric heating rates due to dust extinction. They cleverly reasoned that since the assimilation GCM did not account for dust heating, the increments would include this heating term. At that time the significance of dust contamination on the temperature retrievals was unknown so their approach was sound. Our work shows that before we can determine the dust radiative forcing term from the assimilation temperature increments, the temperature retrievals need correction. On a more general note, the dust contamination of retrievals can lead to unphysical correlations between dust and the quantity retrieved.

[37] We have presented results from a dust correction algorithm for night-time conditions over ocean. During the day and over land, uncertainties in the surface IR emissivity and bi-directional reflectance lead to biases in the assimilation that are much larger than the expected temperature changes from the dust correction. At these times any improvement in the retrievals from the correction are not as consistently apparent as those shown here.

[38] Our retrieval system could be used in an operational mode if model-generated dust concentrations were available. A real-time analysis would be more streamlined with an on-line aerosol transport model. However, before running in operational model, we want to investigate the impact of using SST fields that have been corrected for dust effects [*Nalli and Stowe*, 2002]. The SST fields used in our study are not corrected. Until then, retrievals should be screened where heavy dust loading is suspected. One approach is to use the Aerosol Index (AI), derived solely from TOMS UV radiances, to sense for heavy loading conditions [*Herman et al.*, 1997]. The TOMS AI provides nearly global coverage over both land and ocean back to 1978. Note that MODIS, which uses visible frequencies, cannot see aerosols over the highly reflective Saharan source areas (Figure 1). The current EP-TOMS satellite will be the last in the TOMS satellite series. However, there will be UV instruments on NASA's EOS Aura platform (the Ozone Monitoring Instrument (OMI)) and on future NPOESS satellites that will provide Aerosol Indexes.

[39] **Acknowledgments.** We thank Arlindo da Silva for helpful discussions and assistance with the fvDAS system.

References

Alpert, P., Y. J. Kaufman, Y. Shay-el, D. Tanre, A. daSilva, S. Schubert, and Y. H. Joseph, Dust forcing of climate inferred from correlations between dust data and model errors, *Nature*, *395*, 367–370, 1998.

Aumann, H. H., and R. J. Pagano, Atmospheric Infrared Sounder on the Earth Observing System, *Opt. Eng.*, *33*, 776–784, 1994.

Cohn, S. E., A. M. daSilva, J. Guo, J. Pfaendtner, M. Sienkiewicz, and D. Lamich, Assessing the effects of data selection with the DAO Physical-Space Statistical Analysis System, *Mon. Weather Rev.*, *126*, 2913–2926, 1998.

Diaz, J. P., M. Arbelo, F. J. Exposito, G. Podesta, J. M. Prospero, and R. Evans, Relationship between errors in AVHRR-derived sea surface temperature and the TOMS Aerosol Index, *Geophys. Res. Lett.*, *28*, 1989–1992, 2001.

Ginoux, P., M. Chin, I. Tegen, J. Prospero, B. Holben, and S. Lin, Sources and distributions of dust aerosols simulated with the GOCART model, *J. Geophys. Res.*, *106*, 20,255–20,273, 2001.

Herman, J. R., P. K. Bhartia, O. Torres, C. Hsu, C. Sftor, and E. Celarier, Global distribution of UV-absorbing aerosols from Nimbus 7/TOMS data, *J. Geophys. Res.*, *102*, 16,911–16,922, 1997.

Joiner, J., Investigation of systematic errors and correction models, paper presented at Ninth International TOVS Study Conference, Radiat. Comm. of the Int. Assoc. of Meteorol. and Atmos, *Sci., Igls, Austria*, 1997.

Joiner, J., and L. Rokke, Variational cloud-clearing with TOVS data, *Q. J. R. Meteorol. Soc.*, *126*, 725–748, 2000.

Kiehl, J. T., J. J. Hack, G. B. Bonan, B. A. Boville, B. P. Briegleb, D. L. Williamson, and P. J. Rasch, Description of the NCAR Community Climate Model (CCM3), *NCAR Tech. Note NCAR/TN-420 + STR*, 152 pp., Natl. Cent. for Atmos. Res., Boulder, Colo., 1996.

Lin, S.-J., A finite-volume integration method for computing pressure gradient forces in general vertical coordinates, *Q. J. R. Meteorol. Soc.*, *123*, 1749–1762, 1997.

Lin, S.-J., and R. B. Rood, Multidimensional Flux Form Semi-Lagrangian Transport schemes,, *Mon. Weather Rev.*, *124*, 2046–2070, 1996.

Lin, S.-J., and R. B. Rood, An explicit flux-form semi-Lagrangian shallow water model on the sphere, *Q. J. R. Meteorol. Soc.*, *123*, 2477–2498, 1997.

Lin, S.-J., and R. B. Rood, A flux-form semi-Lagrangian general circulation model with a Lagrangian control-volume vertical coordinate, paper presented at Rossby-100 Symposium, Dep. of Meteorol., Stockholm Univ., Stockholm, 1998.

Masuda, K., T. Takashima, and Y. Takayama, Emissivity of pure and sea waters for the model sea surface in the infrared window regions, *Remote Sens. Environ.*, *24*, 313–329, 1988.

May, D., L. L. Stowe, J. D. Hawkins, and E. P. McClain, A correction for Saharan dust effects on satellite sea-surface temperature-measurements, *J. Geophys. Res.*, *97*, 3611–3619, 1992.

Nalli, N. R., and L. L. Stowe, Aerosol correction for remotely sensed sea surface temperatures from the National Oceanic and Atmospheric Administration advanced very high resolution radiometer, *J. Geophys. Res.*, *107*(C10), 3172, doi:10.1029/2001JC001162, 2002.

Querry, M. R., Optical constants of minerals and other materials from the millimeter to the UV, *Rep. CRDEC-CR-88009*, U.S. Army, Aberdeen, Md, 1987.

Reynolds, W. R., and T. M. Smith, Improved global sea surface temperature analyses using optimum interpolation, *J. Clim.*, *7*, 929–945, 1994.

Schubert, S. R., R. B. Rood, and J. Pfaendtner, An assimilated dataset for Earth science applications, *Bull. Am. Meteorol. Soc.*, *74*, 2331–2342, 1993.

Smith, W. L., H. M. Woolf, C. M. Hayden, D. Q. Wark, and L. M. McMillin, The TIROS-N Operational Vertical Sounder, *Bull. Am. Meteorol. Soc.*, *58*, 1177–1187, 1979.

Sokolik, N., and O. B. Toon, Incorporation of mineralogical composition into models of the radiative properties of mineral aerosol from UV to IR wavelengths, *J. Geophys. Res.*, *104*, 9423–9444, 1999.

Susskind, J., J. Rosenfield, and D. Reuter, An accurate radiative transfer model for use in the direct physical inversion of HIRS and MSU temperature sounding data, *J. Geophys. Res.*, *88*, 8550–8568, 1983.

Weaver, C. J., P. Ginoux, N. C. Hsu, M. Chou, and J. Joiner, Radiative forcing of Saharan dust: GOCART model simulations compared with ERBE data, *J. Atmos. Sci.*, *59*, 736–747, 2002.

P. Ginoux and C. J. Weaver, GEST/University of Maryland, Baltimore County, NASA Goddard Space Flight Center, Code 916, Greenbelt, MD 20771, USA. (ginoux@rondo.gsfc.nasa.gov; weaver@demeter.gsfc.nasa.gov)

J. Joiner, NASA Goddard Space Flight Center, Code 910, 3 GSFC, Greenbelt, MD 20771, USA. (joiner@dao.gsfx.nasa.gov)

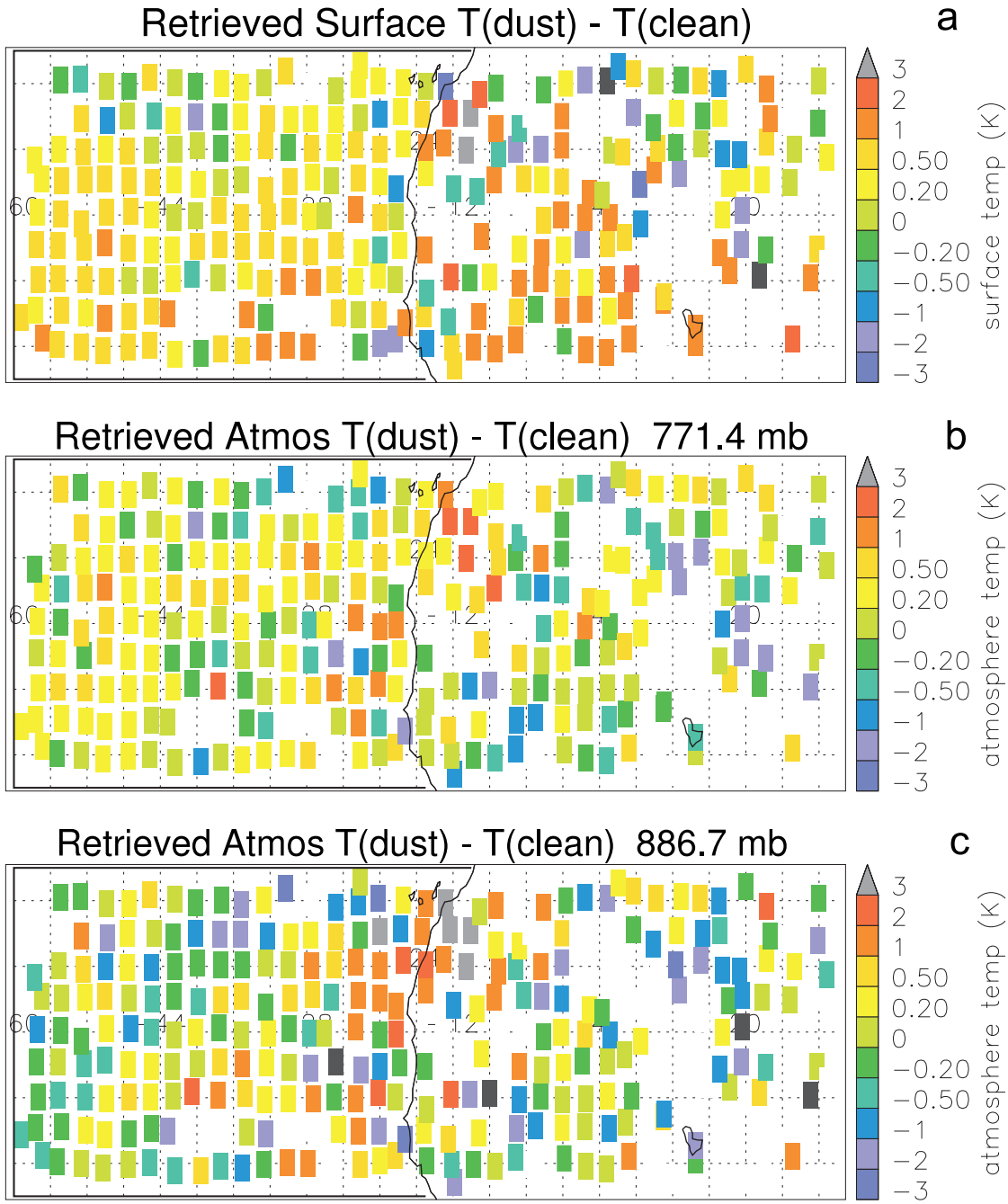

Figure 10. Difference between retrieved temperature from an fvDAS assimilation that accounts for dust minus retrieved temperature from standard assimilation that does not account for dust at (a) surface, (b) 886 hPa, and (c) 771 hPa. Each box represents a time average of temperature retrievals from NOAA-14 sounded from 2–10 June 2001 at 3am local time.